Model Predictive Control in buildings with thermal and visual comfort constraints

Khosravi, M.; Huber, Benjamin; Decoussemaeker, Antoon; Heer, Philipp; Smith, Roy S.

DOI
10.1016/j.enbuild.2023.113831

Publication date
2024

Document Version
Final published version

Published in
Energy and Buildings

Energy & Buildings 306 (2024) 113831

Contents lists available at ScienceDirect

Energy & Buildings

journal homepage: www.elsevier.com/locate/enbuild

Model Predictive Control in buildings with thermal and visual comfort constraints ☆

Mohammad Khosravi [a,*], Benjamin Huber [b], Antoon Decoussemaeker [b,c], Philipp Heer [b], Roy S. Smith [c]

[a] Delft Center for Systems and Control, Delft University of Technology, Delft, Netherlands
[b] Urban Energy Systems Laboratory, Swiss Federal Laboratories for Materials Science and Technology, Empa Dübendorf, Switzerland
[c] Automatic Control Laboratory, Swiss Federal Institute of Technology, ETH Zürich, Switzerland

ARTICLE INFO

Keywords:
Model predictive control
Data predictive control
Building energy
Thermal comfort
Visual comfort
Daylight glare probability

ABSTRACT

Model Predictive Control can cope with conflicting control objectives in building energy managements. In terms of user satisfaction, visual comfort has been proven in several studies to be a crucial factor, however thermal comfort is typically considered the only important aspect. Besides human well-being, visual comfort strongly impacts the productivity of the occupants in offices. Therefore, from an economic point of view, it is essential to include visual comfort in Model Predictive Control for buildings. In this paper semi-linear support vector machine is applied to learn suitable models for visual comfort measured by Daylight Glare Probability. The resulting model is incorporated into a Model Predictive Control framework, together with an autoregressive exogenous model accounting for the thermal dynamics of the building. The approach is validated through an extensive numerical case study, and the benefits of including visual comfort and blind control in the Model Predictive Control problem are evaluated. We observe that the proposed Model Predictive Control scheme ensures both the thermal and visual comfort constraints at the expense of 2.2% to 7.2% higher energy consumption compared to the benchmark Model Predictive Control configuration, which considers only the thermal comfort constraints.

1. Introduction

Buildings account for approximately 40% of the global energy consumption. About half of this energy is allocated to space heating and cooling, ventilation, and air conditioning [1]. On the other hand, people spend around 85% of their lifetime in buildings [2]. Therefore, preserving high quality indoor conditions is crucial for human well-being. Moreover, in non-residential buildings human well-being has also an economic aspect since productivity correlates with comfort [3]. Consequently, improving the energy efficiency of buildings needs to be achieved without compromising the occupant comfort. To this end, various control methodologies are designed to optimize the performance of heating, ventilation, and air conditioning (HVAC) systems [4], including Model Predictive Control (MPC) approaches, which employ a mathematical model of the plant and repetitively solve a constrained optimization problem to find the sequence of optimal control inputs. Since MPC is an appropriate control strategy to suitably balance between conflicting goals, the approach was investigated intensively in research on building automation and control systems [5–11]. For example, [5] deploys a first-principle based MPC in an office building to control the blinds, ventilation, and thermally activated building systems (TABS), and meanwhile, maintain the thermal comfort in the indoor space. Due to the high performance of the building MPC, it has been extended to the data-driven settings [12–15] and distributed scenarios [16].

While typically room temperature and the indoor air quality are considered to quantify user comfort in buildings, the visual conditions also impact the satisfaction and well-being of the occupants, and consequently, their productivity [3]. Accordingly, visual comfort maintenance is proposed to be considered in various shading control strategies [17–19]. Despite the fact that thermal comfort has a relatively standard definition based on indoor temperatures [20], which are well-defined physical quantities that are directly measured with temperature sensors, visual comfort has a human-centric nature that depends on the glare

☆ This research is partially supported from the Swiss National Science Foundation for the first author [Postdoc.Mobility Grant 211104].
* Corresponding author.
E-mail addresses: mohammad.khosravi@tudelft.nl (M. Khosravi), benjamin.huber@empa.ch (B. Huber), antoon_96@hotmail.ch (A. Decoussemaeker), philipp.heer@empa.ch (P. Heer), rsmith@control.ee.ethz.ch (R.S. Smith).

https://doi.org/10.1016/j.enbuild.2023.113831
Received 31 July 2023; Received in revised form 31 October 2023; Accepted 13 December 2023
Available online 28 December 2023

Fig. 1. NEST demonstrator with the office unit SolAce on the right side of the second floor (red box) [26]. (For interpretation of the colors in the figure(s), the reader is referred to the web version of this article.)

perception by the users. Nevertheless, some rather ad-hoc approaches are employed in the literature to include the visual comfort inside buildings [21]. To correctly assess the excess glare inside a building, a specific index called *Daylight Glare Probability* (DGP) is experimentally developed based on factors such as luminance, solid angle, and position index of the glare sources [22]. The strong correlation between DGP and perceived glare, which is verified through the feedback of users, has made DGP a relatively standardized metric for visual comfort despite its heavily complex definition. Considering this feature of DGP, a building MPC scheme with thermal and visual comfort is proposed in [23], where white-box modeling approaches are employed to obtain the value of DGP and the thermal dynamics of the building. According to the complexity of DGP definition, white-box and parametric modeling approaches for DGP, like those utilized in [23], demand exhaustive parameter estimation and significant model tuning. In general, while data-driven modeling frameworks, like black-box techniques, are comparably scalable and independent of specific modeling expertise, physics-based paradigms, such as white-box and gray-box schemes, are based on expert knowledge and may result in either excessively simplistic models or intractable parameter estimations [24]. Due to this fact and since the direct calculation of DGP is rather challenging, advanced calibrated sensing devices have been recently designed to ease measuring DGP and provide proper assessment of visual comfort [25]. The existing building MPC approaches either do not take into account visual comfort [5,10], or, it is considered independently from the thermal energy concerns [19], or, their consideration is not based on proper standard metrics like DGP [21], or, they employ intractable and unscalable modeling approaches for DGP with prohibitive calibration and parameter tuning load [23].

Following the discussion above, this work addresses the indicated gap in the literature by proposing a suitable MPC scheme with proper consideration of thermal and visual comfort where data-driven modeling approaches are employed for building thermal dynamics and DGP. Note that satisfying thermal and visual comfort while reducing the energy consumption is a challenging and conflicting task as solar irradiation is a source of free thermal energy but may also violate visual comfort, i.e., independent operation of heating and shading systems leads to sub-optimal overall performance. Accordingly, we need to resolve the following challenges:

- How can we design a building MPC with *both* thermal and visual comfort inclusion?
- How can we ensure the tractability of the MPC formulation?
- What are the potential savings and costs in terms of energy and comfort violations?

To address these questions, we develop an MPC scheme based on a linear *autoregressive exogenous* (ARX) model of the thermal dynamics and a semi-linear *support vector regression* (SVR) model for predicting DGP. Furthermore, we evaluate the proposed scheme on a numerical case study derived through measurement data from the SolAce apartment in NEST, a district scale living lab located in Dübendorf, Zürich, Switzerland, shown in Fig. 1.

Table 1
Nomenclature.

DGP	Daylight Glare Probability
MPC	Model Predictive Control
MPC-TC&VC	MPC with thermal and visual comfort constraints
MPC-NB	MPC with thermal comfort constraints and no blind control
MPC-TC	MPC with thermal comfort constraints
MPC-VC&TLB	MPC with visual comfort and thermal lower bound constraints
PRBS	Pseudo-Random Binary Signals
RBC	Rule-Based Control
RBC-SB	RBC with night temperature setback
SVM	Support Vector Machine

The remainder of this paper is structured as follows: In Section 2, we cover the main challenges to be addressed in the proposed MPC, which is thoroughly explained in Section 3. Section 4 describes the simulated building and the numerical case study. The results of the case study are presented and discussed in Section 5. Finally, Section 6 concludes the paper and provides the outlook on future research directions. The abbreviations and notation used in this paper are provided in Table 1 and Table 2, respectively.

2. Model predictive control of buildings: visual comfort challenge

MPC is an online control strategy that provides near optimal decisions resulting in maximal utilization of the energy system in buildings including considered constraints. The MPC excellent performance is due to the joint consideration of energy minimization and comfort satisfaction. The main advantage of MPC is due to its potential in taking into account the operational and technological limitations, the forecasts of weather and climate variables, and the thermal dynamics of the building. In the implementation of MPC, the time axis is discretized based on a suitable sampling period, and, an optimization problem is solved at each discrete time-step k to obtain a sequence of optimal decisions $\mathrm{u}^* := (u_0^*, \dots, u_{N-1}^*)$, where N is the planing horizon. Following this, the first control input, u_0^*, is applied to the system, the measurements are updated, and the time horizon is rolled forward. The MPC optimization problem has the following generic form

$$\underset{\mathrm{x},\mathrm{u}}{\text{minimize}} \quad J(\mathrm{x},\mathrm{u}) := \sum_{k=0}^{N-1} \ell_k(x_k, u_k) + \ell_N(x_N) \tag{1a}$$

$$\text{subject to} \quad x_{k+1} = f(x_k, u_k, d_k), \quad k = 0, \dots, N-1, \tag{1b}$$

$$u_k \in \mathcal{U}_k, \qquad k = 0, \dots, N-1, \tag{1c}$$

$$x_k \in \mathcal{X}_k, \qquad k = 1, \dots, N, \tag{1d}$$

where x_0 is the given initial state, $\mathrm{u} := (u_0, \dots, u_{N-1})$, $\mathrm{x} := (x_1, \dots, x_N)$, and $\mathrm{d} := (d_0, \dots, d_{N-1})$ are respectively the inputs, the states, and the disturbances over the MPC horizon, f describes the thermal dynamics of the building, $\ell_0, \dots, \ell_{N-1}$ are running cost functions, ℓ_N is the terminal cost function, and, $\mathcal{U}_0, \dots, \mathcal{U}_{N-1}$ and $\mathcal{X}_1, \dots, \mathcal{X}_N$ are the sets of admissible inputs and states, respectively. Though (1b) is a state-space representation, it can be an input-output description for the building thermal dynamics, such as an ARX model [24], which is more common in the practical implementation of building MPC as the hidden states are often not constrained. Additionally, the disturbances $\mathrm{d} = (d_0, \dots, d_{N-1})$ encapsulate the climate variables or their predicted values for the subsequent N time steps. The operational limitations and practical constraints on the inputs are considered through the constraint sets $\mathcal{U}_0, \dots, \mathcal{U}_{N-1}$. On the other hand, since the states are typically temperatures of the zones, $\mathcal{X}_1, \dots, \mathcal{X}_N$ primarily characterize the thermal

Table 2
Notation.

x_k	state variables (temperatures) at k
u_k	inputs or decision variables (heating powers and blind positions) at time k
d_k	disturbances (climate variables) at time k
f	thermal dynamics of the building
N	horizon of MPC
x	vector of all states over the MPC horizon
u	vector of all inputs over the MPC horizon
d	vector of all disturbances over the MPC horizon
ℓ_k	running cost of MPC for time k
ℓ_N	terminal cost of MPC
$\mathcal{X}_k$	state constraints at time k
$\mathcal{U}_k$	input constraints at time k
$\mathcal{Z}_k$	visual comfort constraints at time k
T	(generic) temperature variable
T_k	temperature (of the zone) at time k
$T_k^{\min}$	temperature upper bound for thermal comfort at time k
$T_k^{\max}$	temperature lower bound for thermal comfort at time k
$\mathrm{DGP}_{\max}$	DGP bound for visual comfort
$\dot{Q}$	total heat flow
m	lumped mass of the thermal zone
c_p	specific heat capacity
$\dot{Q}^{(\mathrm{amb})}$	heat flow from the ambient space
κ_{amb}	heat transfer coefficient between zone and ambient space
A_{amb}	surface area between zone and ambient space
$T_k^{(\mathrm{amb})}$	ambient temperature at time k
N_{adj}	number of adjacent zones
$\dot{Q}^{(\mathrm{adj})}$	heat flow from the adjacent zones
$\kappa_{\mathrm{adj},i}$	heat transfer coefficient between zone and i^{th} adjacent zone
$A_{\mathrm{adj},i}$	surface area between zone and i^{th} adjacent zone
$T_k^{(\mathrm{adj},i)}$	temperature of i^{th} adjacent zone at time k
$\dot{Q}^{(\mathrm{sol})}$	heat flow from the solar irradiation
I_{hor}	global irradiation on a horizontal plane
A_{win}	window area
ϕ_{bl}	fraction of the window area shaded by the blinds
α_{win}	orientation of the window
α	azimuth angle of the sun
β	elevation angle of the sun
$\dot{Q}^{(\mathrm{heat})}$	heat flow from the heating system
$T^{(\mathrm{s})}$	temperature of supply water in the heating system
$T^{(\mathrm{r})}$	temperature of return water in the heating system
$\dot{m}^{(\mathrm{flow})}$	mass flow of water in the pipes
E_{v}	vertical eye illuminance experienced by the user
n_{gs}	number of glare sources
L_i	luminance for the i^{th} source of glare
ω_i	solid angle for the i^{th} source of glare
P_i	position index for the i^{th} source of glare
$\theta^{(\cdot)}, \boldsymbol{\theta}^{(\cdot)}$	ARX coefficients/vectors for the respective variables
$f_{\mathrm{DGP}}, c_{\mathrm{DGP}}$	DGP regression and classification models

comfort constraints, which can be softened and relaxed by introducing slack variables. This also ensures the feasibility of optimization problem (1). The tractability of (1) can be guaranteed by the convexity that is implied by the linearity of f in (1b) and the convexity of the cost function J in (1a), and the sets $\mathcal{U}_0, \dots, \mathcal{U}_{N-1}$ and $\mathcal{X}_1, \dots, \mathcal{X}_N$ respectively in (1c) and (1d).

In order to incorporate visual comfort in the building MPC, we need to modify (1) by including additional suitably designed terms and constraints indicating the potential excessive perceptible glares in the indoor environment. While thermal comfort has a standardized definition based on well-defined physical quantities [20], i.e., the temperature of the zones, which are the state variables of the system and measured directly using temperature sensors, the notion of visual comfort is a human-centered concept and defined based on a specifically designed index called *Daylight Glare Probability* (DGP) [22], which is a complicated metric and demands particular advanced optical measurement devices. Accordingly, incorporating visual comfort into the building MPC is comparably more challenging and not straightforward. More precisely, we need to address the following questions:

1. How can we modify (1) to incorporate the visual comfort, based on the DGP index, together with the thermal aspects of the problem?
2. What is an efficient way of learning DGP from measurement data?
3. How can we ensure that the obtained DGP model is suitable for the MPC implementation?
4. To what extent and how should one compromise between thermal and visual comforts versus energy consumption, and what is the subsequent outcome regarding overall energy usage?

To address the first question, we may use a similar approach to the consideration of thermal comfort. More precisely, we need to modify (1) by introducing suitable constraints for the inclusion of visual comfort, which characterize admissible positions of blinds based on the perceived glare from solar radiation. Accordingly, the additional constraints should be in the following form

$$(u_k, d_k) \in \mathcal{Z}_k, \qquad k = 0, \dots, N-1, \tag{2}$$

where sets $\mathcal{Z}_0, \dots, \mathcal{Z}_{N-1}$ are defined based on the learned model of DGP. Thus, we need to take care of the efficient characterization of these sets and the tractability of subsequently formulated MPC, which are the main concerns highlighted by questions 2 and 3 above. Further formulation details and discussions on addressing the above questions are given in the following sections, where we explain the MPC approach proposed in this work and compare it with scenarios without shading control or visual comfort constraints.

3. Model predictive control with thermal and visual comfort

This section introduces the proposed building MPC with thermal and visual comfort considerations. To this end, we need to modify (1), and elaborate on deriving the necessary terms in (1) and (2). The main concern is obtaining a correct and meanwhile tractable MPC formulation.

3.1. Thermal dynamics and comfort in building

Using first principles to model the thermal dynamics of a building is a tedious procedure. Since buildings are unique in terms of construction, location, and operation, an individual model needs to be identified for each building. On the other hand, conventional learning methods require a significant amount of informative data to achieve reasonable accuracy and be physically meaningful. Accordingly, we employ a data-driven modeling strategy that substantially reduces the model learning effort. Nevertheless, the model structure and inputs are inspired by the first principles and physical laws. By that, the data efficiency is improved considerably compared to conventional learning methods [11].

Following the first law of thermodynamics, stating that energy is conserved in a closed system, we can define the system boundaries of the building accordingly, and take into account only a single state by lumping the mass of the modeled thermal zone into one parameter m. Consequently, the thermal dynamics of the building is as follows

$$m\, c_p \frac{\mathrm{d}T}{\mathrm{d}t} = \dot{Q}^{(\mathrm{amb})} + \dot{Q}^{(\mathrm{adj})} + \dot{Q}^{(\mathrm{int})} + \dot{Q}^{(\mathrm{sol})} + \dot{Q}^{(\mathrm{heat})} =: \dot{Q}, \tag{3}$$

where c_p is the specific heat capacity, T denotes the temperature of the zone, and $\dot{Q}$ is the total heat flow between the controlled zone and its environment, which consists of the net heat coming from the ambient

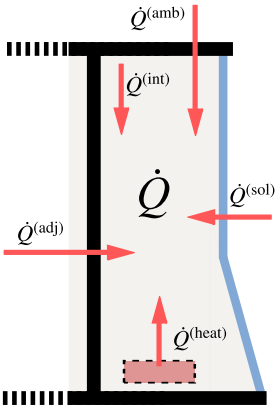

Fig. 2. Different sources of heat flow in the case study building.

space, $\dot{Q}^{(\mathrm{amb})}$, the adjacent zones, $\dot{Q}^{(\mathrm{adj})}$, the solar irradiation, $\dot{Q}^{(\mathrm{sol})}$, the internal heat gains, $\dot{Q}^{(\mathrm{int})}$, and, the heating system, $\dot{Q}^{(\mathrm{heat})}$ (see Fig. 2). The heat flow between the considered thermal zone and the ambient space can be described by

$$\dot{Q}^{(\mathrm{amb})} = \kappa_{\mathrm{amb}}\, A_{\mathrm{amb}}\, \left(T^{(\mathrm{amb})} - T\right), \tag{4}$$

where κ_{amb} is the heat transfer coefficient, A_{amb} is the surface area, and $T^{(\mathrm{amb})}$ is the ambient temperature. Similarly, for the impact of adjacent thermal zones, we have

$$\dot{Q}^{(\mathrm{adj})} = \sum_{i=1}^{N_{\mathrm{adj}}} \kappa_{\mathrm{adj},i}\, A_{\mathrm{adj},i}\, \left(T^{(\mathrm{adj},i)} - T\right), \tag{5}$$

where N_{adj} denotes the number of adjacent zones, and, for $i = 1, \ldots, N_{\mathrm{adj}}$, the heat transfer coefficient, the surface area, and the temperature for the i^{th} adjacent zone are denoted respectively by $\kappa_{\mathrm{adj},i}$, $A_{\mathrm{adj},i}$, and $T^{(\mathrm{adj},i)}$. The internal heat gains $\dot{Q}^{(\mathrm{int})}$, caused by occupancy and appliances, are commonly neglected according to their random nature and the difficulty in their modeling and prediction. The solar gain $\dot{Q}^{(\mathrm{sol})}$ is mainly due to the irradiation entering the room through the windows. Given the measurement of the global irradiation on a horizontal plane, I_{hor}, the solar gain can be obtained as

$$\dot{Q}^{(\mathrm{sol})} = \phi_{\mathrm{bl}}\, A_{\mathrm{win}}\, \sin(\alpha - \alpha_{\mathrm{win}})\, \cot(\beta)\, I_{\mathrm{hor}}, \tag{6}$$

where A_{win} is the window area, α_{win} is the orientation of the window, $\phi_{\mathrm{bl}} \in [0, 1]$ is the fraction of the window area shaded by the blinds, and, α and β are respectively the azimuth and the elevation angles of the sun. The gains from the heating system $\dot{Q}^{(\mathrm{heat})}$ can be described as

$$\dot{Q}^{(\mathrm{heat})} = \dot{m}^{(\mathrm{flow})}\, c_p\, (T^{(\mathrm{s})} - T^{(\mathrm{r})}), \tag{7}$$

where $\dot{m}^{(\mathrm{flow})}$ denotes the mass flow of water in the pipes, c_p the specific heat capacity of water, and, $T^{(\mathrm{s})}$ and $T^{(\mathrm{r})}$ are respectively supply and return temperature. Accordingly, by substituting terms in (4), (5), (6) and (7) in the right-hand side of (3), and employing Euler discretization, we have

$$\begin{aligned} T_{k+1} = \theta T_k + \theta^{(\mathrm{amb})} T_k^{(\mathrm{amb})} + \sum_{i=1}^{N_{\mathrm{adj}}} \theta^{(\mathrm{adj},i)} T_k^{(\mathrm{adj},i)} + \theta^{(\mathrm{sol})} \dot{Q}_k^{(\mathrm{sol})} \\ + \theta^{(\mathrm{heat})} \dot{Q}_k^{(\mathrm{heat})}, \end{aligned} \tag{8}$$

where k denotes the discrete time index, and θ, $\theta^{(\mathrm{amb})}$, $\theta^{(\mathrm{adj},1)}, \ldots, \theta^{(\mathrm{adj},N_{\mathrm{adj}})}$, $\theta^{(\mathrm{sol})}$ and $\theta^{(\mathrm{heat})}$ are the coefficients characterizing the impact of corresponding terms.

While model (8) is based on the first-principles, it disregards the thermal inertial caused by the heat potential preserved in the mass of the building. To include this attribute in the building thermal dynamics, we extend (8) to a linear *autoregressive exogenous* (ARX) model [24] with similar structure, i.e., (8) is modified by considering further history of the temperature measurements. Thus, the model acquires more information about the system dynamics and captures indirectly unmeasured inputs and hidden states, such as the temperature of the walls, ceilings and floors. Moreover, as the model is inspired by the first-principles, it is physically consistent and interpretable. The generic ARX model has the following form

$$x_{k+1} = \sum_{j=0}^{n_x} a_j\, x_{k-j} + \sum_{j=0}^{n_u} b_j\, u_{k-j} + e_k, \tag{9}$$

where x_k and u_k respectively denote the state signal and exogenous input at time k, n_x and n_u are the number of lags used in the ARX model respectively for state and input, $a_0, \ldots, a_{n_x}$ and $b_0, \ldots, b_{n_y}$ are the coefficients characterizing the model by determining the impact of corresponding lag of state or input, and, e_k is the uncertainty term [24]. According to the discussion above and inspired by the first-principles based model (8), the thermal dynamics of the building can be formulated as the following ARX model

$$\begin{aligned} T_{k+1} = \sum_{j=0}^{n_T} \theta_j\, T_{k-j} + \sum_{j=0}^{n_{\mathrm{amb}}} \theta_j^{(\mathrm{amb})}\, T_{k-j}^{(\mathrm{amb})} + \sum_{i=1}^{N_{\mathrm{adj}}} \sum_{j=0}^{n_{\mathrm{adj},i}} \theta_j^{(\mathrm{adj},i)}\, T_{k-j}^{(\mathrm{adj},i)} \\ + \sum_{j=0}^{n_{\mathrm{sol}}} \theta_i^{(\mathrm{sol})}\, \dot{Q}_{k-j}^{(\mathrm{sol})} + \sum_{j=0}^{n_{\mathrm{heat}}} \theta_j^{(\mathrm{heat})}\, \dot{Q}_{k-j}^{(\mathrm{heat})} + e_k, \end{aligned} \tag{10}$$

which is a generalized form of (8). Using the measurement data and the least-squares regression, we can estimate the coefficients of ARX model (10). More details are provided in Appendix A.

Remark 1. To account for the impact of potential nonlinearities, such as those emanating from the valves in the heating system, one may employ nonlinear models for the building thermal dynamics, e.g., in the form of a Hammerstein-Wiener system [24]. While the resulting models can offer a closer approximation to reality, they are not suitable for efficient implementation of MPC, i.e., their inclusion in the optimization problem (1) introduces nonconvexity and consequently leads to tractability issues. Nevertheless, these more accurate nonlinear models can serve as a reference representing the actual thermal dynamics of the building in numerical experiments, as is the case in this study.

Remark 2. The accuracy of (10) can be improved by including the impact of internal gains and occupants, which are intrinsically of a random nature. Accordingly, to avoid dealing with an over-complicated model, we primarily employ the building thermal dynamics introduced in (10).

The thermal comfort in the building has a relatively standard definition based on indoor temperatures [20]. More precisely, it is said that the controlled zone achieves thermal comfort if its room temperature at time instant k fulfills

$$T_k^{\min} \le T_k \le T_k^{\max}, \tag{11}$$

where $T_k^{\min}$ and $T_k^{\max}$ are given specific bounds, which can depend on the ambient temperature. It is worth noting that (11) is commonly treated as a soft constraint in the building MPC, i.e., (11) is relaxed using slack variables to guarantee the feasibility for optimization problem in MPC and improve its tractability.

3.2. Visual comfort modeling and assessment

The notion of visual comfort depends on several factors, including deterministic physical quantities such as luminance, solid angle, and position index of the glare sources. Meanwhile, due to its human-centric nature and user-perceived subjectivity, it exhibits characteristics of randomness. Accordingly, any suitably designed visual comfort index is

Fig. 3. DGP measurement device.

expected to have a probabilistic form defined based on measured related physical quantities. In the literature, *Daylight Glare Probability* (DGP) is proposed as the standardized metric [22], specifically designed to indicate the chance of experiencing excessive glare. More precisely, DGP quantifies the probability that a typical user perceives disturbing amount of glare based on vertical eye illuminance and parameters of glare sources. Through empirical and field studies [22], the mathematical description of DGP is obtained as follows

$$\mathrm{DGP} = \frac{5.87}{10^5} E_{\mathrm{v}} + \frac{9.18}{10^2} \log\left(1 + \sum_{i=1}^{n_{\mathrm{gs}}} \frac{L_i^2 \omega_i}{E_{\mathrm{v}}^{1.87} P_i^2}\right), \tag{12}$$

where E_{v} [lux] is the vertical eye illuminance experienced by the user, n_{gs} denotes the number of glare sources, and, L_i [cd/m^2], ω_i and P_i are respectively the luminance, solid angle and position index for the i^{th} source of glare, for $i = 1, \dots, n_{\mathrm{gs}}$. Note that the DGP value obtained from (12) practically belongs to interval $[0, 1]$, which is consistent with its notion. Moreover, from an empirical perspective, (12) indicates approximately the ratio of users which are possibly visually uncomfortable. Accordingly, the visual comfort constraint is defined as follows

$$\mathrm{DGP} \le \mathrm{DGP}_{\max}, \tag{13}$$

where $\mathrm{DGP}_{\max} \in [0, 1]$ is a suitably chosen upper bound. To verify (13), we need to evaluate DGP using (12), and thus, the values of above-mentioned quantities are required. Needless to say, detecting each of the different glare sources and obtaining the corresponding quantities is a prohibitive manual routine. Accordingly, an advanced well-calibrated device has been designed in [19,25], and performs this procedure in a fully automated way, i.e., it directly outputs the value of DGP. The device is shown in Fig. 3.

The value of DGP depends on solar variables and blinds position through the quantities describing glaring sources in (12), including E_{v} and L_i, ω_i, P_i, for $i = 1, \dots, n_{\mathrm{gs}}$. While DGP can be efficiently measured, the dependency of these quantities to the solar variables and blinds position has a complex black-box form. More precisely, while one can measure DGP for different status of blind position and solar radiation, the rule describing DGP as a function of these variables is not given. Since in building MPC, one can control blinds and predict climate variables, it is desired to obtain DGP as function $f_{\mathrm{DGP}} : \mathcal{U}^{(\mathrm{bld})} \times \mathcal{D}^{(\mathrm{sol})} \to [0, 1]$, where $\mathcal{U}^{(\mathrm{bld})}$ denotes the set for admissible positions of blinds $u^{(\mathrm{bld})}$ and $\mathcal{D}^{(\mathrm{sol})}$ is the set characterizing the range of solar variables $d^{(\mathrm{sol})}$. Then, the visual comfort (13) can be considered in the MPC problem by including the following constraints

$$f_{\mathrm{DGP}}(u_k^{(\mathrm{bld})}, d_k^{(\mathrm{sol})}) \le \mathrm{DGP}_{\max}, \quad k = 0, \dots, N-1, \tag{14}$$

in the MPC optimization problem (1). Given a set of measurement data as follows

$$\mathscr{D} := \left\{ (u_i^{(\mathrm{bld})}, d_i^{(\mathrm{sol})}, \mathrm{DGP}_i) \,\middle|\, i = 1, \dots, n_{\mathscr{D}} \right\}, \tag{15}$$

where $n_{\mathscr{D}}$ denotes the number of data points, we can learn the DGP function f_{DGP} with high accuracy using various readily available non-linear regression methods [27]. However, since the resulting function can be quite complex and non-convex, it will not be suitable for the MPC implementation. Alternatively, one may employ a classification framework. Accordingly, for $i = 1, \dots, n_{\mathscr{D}}$, we label the i^{th} measurement data point as l_i, with $l_i = -1$, when $\mathrm{DGP}_i \le \mathrm{DGP}_{\max}$, and $l_i = 1$, when $\mathrm{DGP}_i > \mathrm{DGP}_{\max}$. Thus, l_i indicates whether DGP_i violates the visual comfort bound. Subsequently, we learn a classifier map $c_{\mathrm{DGP}} : \mathcal{U}^{(\mathrm{bld})} \times \mathcal{D}^{(\mathrm{sol})} \to \{-1, 1\}$, to be employed later in the MPC optimization problem. For the efficient implementation of MPC, we need a convex formulation. Accordingly, we employ a semi-linear *support vector machine* (SVM) which is a slightly modified version of standard linear SVM [28]. More precisely, for any $u^{(\mathrm{bld})} \in \mathcal{U}^{(\mathrm{bld})}$ and $d^{(\mathrm{sol})} \in \mathcal{D}^{(\mathrm{sol})}$, we define function c_{DGP} as

$$c_{\mathrm{DGP}}(u^{(\mathrm{bld})}, d^{(\mathrm{sol})}) = \mathrm{sign}(w^{\mathsf{T}} \begin{bmatrix} u^{(\mathrm{bld})} \\ \Psi(d^{(\mathrm{sol})}) \end{bmatrix} - b), \tag{16}$$

where $\mathrm{sign}(\cdot)$ denotes the sign function, $\Psi(\cdot)$ is a given nonlinear transformation lifting $d^{(\mathrm{sol})}$ to a space of higher dimension, vector w and real scalar b are obtained from solving the following convex optimization

$$\begin{aligned} &\min_{w,b} \ \|w\|^2 + \gamma \sum_{i=1}^{n_{\mathscr{D}}} \zeta_i^2, \\ &\text{s.t.} \ \ l_i(w^{\mathsf{T}} \begin{bmatrix} u_i^{(\mathrm{bld})} \\ \Psi(d_i^{(\mathrm{sol})}) \end{bmatrix} - b) \ge 1 - \zeta_i, \ i = 1, \dots, n_{\mathscr{D}}, \\ &\quad \zeta_i \ge 0, \qquad\qquad\qquad\qquad i = 1, \dots, n_{\mathscr{D}}, \end{aligned} \tag{17}$$

and, γ is a positive real hyperparameter employed for tuning the soft-margin of the classifier and to ensure the uniqueness of solution for (17). Following this, one can reformulate constraint (13) as $c_{\mathrm{DGP}}(u^{(\mathrm{bld})}, d^{(\mathrm{sol})}) \le 0$. Thus, we can include the visual comfort in the MPC problem (1) through the following equivalent inequalities

$$w^{\mathsf{T}} \begin{bmatrix} u_k^{(\mathrm{bld})} \\ \Psi(d_k^{(\mathrm{sol})}) \end{bmatrix} - b \le 0, \quad k = 0, \dots, N-1. \tag{18}$$

Note that the introduced constraints are linear with respect to optimization variables $u_0^{(\mathrm{bld})}, \dots, u_{N-1}^{(\mathrm{bld})}$, and therefore, convex.

Remark 3. To improve the accuracy of the proposed DGP reformulation, one may first employ clustering techniques [27] to partition the measurement data into subsets containing data points with similar values of $d^{(\mathrm{sol})}$, and subsequently, with respect to each of these sets, learn a classifier map as discussed above.

Remark 4. One can learn more accurate models for DGP using nonlinear classification techniques such as kernel SVM [27]. While the obtained mathematical models may represent reality well, they are not suitable for an efficient implementation of MPC, i.e., their inclusion in optimization problem (1) results in non-convexity and thus intractability. Nonetheless, the mentioned relatively exact nonlinear models can be employed as a reference characterizing the actual DGP perceived by the occupants in the building and can be utilized in numerical studies, as is the case in the current paper.

Remark 5. Given the possibility of measuring the illuminance, one can modify the proposed MPC formulation to ensure sufficient illuminance in the workspace as well. To this end, we need to additionally consider the electricity cost of the lights in the MPC objective function and include constraints ensuring sufficient illuminance throughout the MPC horizon. These constraints may be learned efficiently via an approach similar to the introduced semi-linear support vector machine algorithm.

Remark 6. The thermal dynamics of the building and the perceived glare are both affected by solar radiation. Nonetheless, from the control perspective, they are coupled through the control input that determines the status of blinds. More precisely, while opening the blinds results in

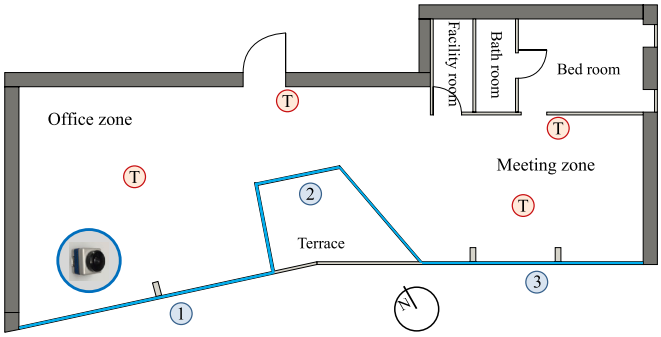

Fig. 4. The figure shows the floor plan of the NEST unit SolAce. The temperature measurement sensors are shown with Ⓣ. The numbers ①, ②, and, ③ refer to the windows.

receiving more solar thermal energy, it may lead to experiencing higher levels of glare and visual discomfort. Accordingly, the task of making the optimal decision and deriving the best trade-off is delegated to the proposed MPC strategy.

4. Numerical experiment case study: SolAce unit

In this section, we provide the technical details of the real-world system that served as the basis for our research study and discuss the framework for our subsequent numerical experiments.

4.1. Building and physical configurations

The simulation model used in this case study originated from the office unit SolAce in the NEST demonstrator [26]. Fig. 1 shows the NEST demonstrator. SolAce[1] is the unit on the right side of the second floor with a blue facade. The floor plan of SolAce is depicted in Fig. 4. SolAce can be considered as a single-room office with a total area of approximately 104 m^2. A small terrace separates the office zone from the meeting zone. Within the unit, water-based heating and cooling panels are mounted on the ceiling. The central heating and cooling system supplies these panels via heat exchangers connected to a network of pipes on both sides. The pipes linking the heat exchangers to the central energy system are equipped with controlled valves and pumps, ensuring a well-regulated water inflow. On the unit side, the pipe network transfers and circulates heated or cooled water through the heat exchangers and the panels, driven by a dedicated pump. Suitably controlled valves determine the flow rate within these pipes. The utilized low-level controllers on both the unit and central energy system sides have PID structures with finely tuned coefficients to precisely adjust the position of valves, flow rates, and supply temperatures. These controllers are designed to track a predefined reference signal generated by the high-level control system, i.e., the employed model predictive control strategy. The windows are mainly oriented towards the southwest, primarily to harness natural daylight and maximize the solar heat gain during the day. Venetian blinds with sinusoidal slats are installed on the exterior side of the windows within the office section of the unit; i.e., the blinds are not located inside the unit. The blinds are equipped with an electric motorized system that precisely adjusts their height and slat angles. These adjustments are performed through a finely tuned tracking PID control scheme with the reference designed by the high-level controller, namely, the model predictive control strategy mentioned above. Given the external placement of the blinds and being endowed with relatively thin, metal-based slats, their status mainly affects the amount of solar radiation entering the unit and, subsequently, the perceived glare and solar thermal gain. The unit is equipped with all necessary measurement

[1] For a virtual tour of the SolAce unit, one can check the following link: https://www.empa-virtual.ch/nest/en/solace/.

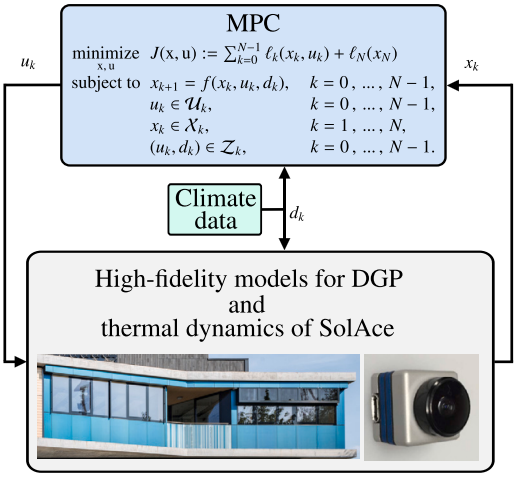

Fig. 5. The figure shows the scheme of numerical experiment using obtained high fidelity models for DGP and the thermal dynamics of SolAce unit at NEST.

devices, including sensors for measuring quantities such as the temperature of the room, the indoor air quality, the blind position, and the energy flows to and from the unit (i.e., heat and electricity). Additionally, the DGP measurement device (see Fig. 3) is installed in the office zone adjacent to the desk to assess the glare experienced by the user while working. The ambient temperature is measured locally by temperature sensors installed on the roof of the NEST building. The height and azimuth angles of the sun, as well as the remaining climate variables, including the global and diffused solar irradiation, are provided by MeteoSwiss. For further information about the SolAce unit, one can check the following link: https://www.empa.ch/web/nest/solace.

4.2. Numerical experiment framework

The scheme of our numerical experiments is shown in Fig. 5. Following our discussion in Section 3, suitable models for the MPC implementation are required, one for the thermal dynamics of the building and one for DGP. Additionally, we need high-fidelity models for these entities to accurately imitate reality in our numerical experiments. To obtain these models, we require informative measurement data that can be collected by performing suitably designed experiments. For the thermal dynamics of the building, appropriately scaled pseudo-random binary signals (PRBS) are applied to the heating system to actuate the system with different possible input combinations. The experiment is repeated under a variety of climate conditions with distinct solar radiation and ambient temperature situations. The aforementioned models are estimated from the collected data and the readily available historical measurements. More precisely, the coefficients of linear ARX model (10) are estimated by solving a least-squares regression problem formulated based on the given temperature and heating measurements. Similarly, we utilize the data to identify a high-fidelity model of the building thermal dynamics as a Hammerstein-Wiener system (see Remark 1). Analogously, to learn the necessary models of DGP, we collect informative data by conducting specifically designed experiments where different combinations of blind position and slat angle are considered in various solar situations. The optimization problem (17) is formulated given the measurement data and solved to obtain the DGP model to be utilized in the MPC implementation. In a similar fashion, the DGP high-fidelity model is learned as a kernel SVM classifier (see Remark 4).

5. Results

This section presents and discusses the results of the numerical experiments in our research study. The main objective is to provide a thorough comparison by analyzing various control scenarios considering

Table 3
Performance comparison for different control schemes including visual comforts.

	Method Acronym	Energy Consumption [kWh]	Thermal UB Violation [Kh]	Thermal LB Violation [Kh]	Visual Violation [h/day]	Blind Closed [h]
RBC	RBC	1804	112	4.42	0.40	195
RBC with night temperature setback	RBC-SB	1442	32.8	327	0.64	169
MPC with thermal and visual comfort constraints	MPC-TC&VC	1663	7.45	49.9	0.07	146

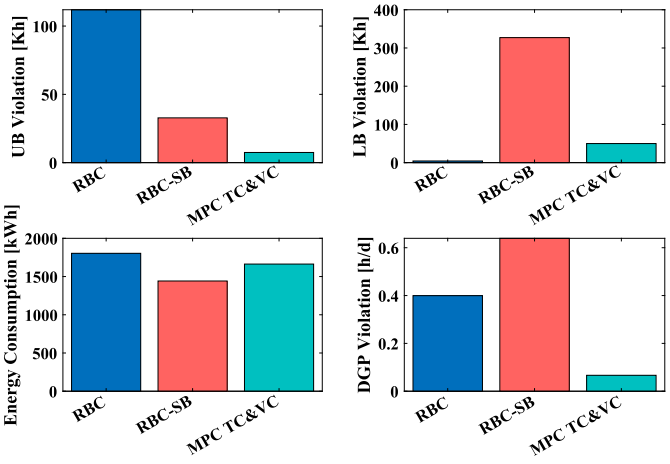

Fig. 6. Performance comparison for different control schemes including visual comforts.

visual comfort concerns. Furthermore, we compare different implementations of Model Predictive Control (MPC), highlighting the potential impact of the visual comfort constraints and roles of the blinds.

5.1. Control schemes with thermal and visual comfort consideration

To investigate and assess the impact of visual comfort constraints on control implementations, we conduct a thorough evaluation of the performance of various building thermal control scenarios where visual comfort is taken into account in addition to the thermal comfort constraints. More precisely, we compare the performance of the following control scenarios:

- *Rule-Based Control* (RBC): This control scheme utilizes a generic hysteresis controller to maintain the temperature of the zone at approximately 23 °C. More specifically, the controller employs two thresholds that determine when to initiate heating and when to stop it. Once the zone temperature falls below the lower threshold, the controller starts heating until the temperature exceeds the upper threshold. Furthermore, if the room temperature is high and a considerable amount of solar radiation is detected, the controller will close the blinds as an additional action.
- *RBC with night temperature setback* (RBC-SB): This case is a modified version of the above mentioned RBC. More precisely, during the night hours, the temperature lower bound is adjusted to a relaxed setting of 20 °C.
- *MPC with thermal and visual comfort constraints* (MPC-TC&VC): This is the scenario discussed in the present paper, namely the MPC implementation, which takes into account both thermal and visual comfort constraints.

Table 3 and Fig. 6 compare the control performance for the schemes mentioned above. Moreover, Fig. 7 illustrates the room temperatures and the amount of perceived glare over the course of five days, showcasing the outcomes of utilizing the aforementioned control schemes.

Discussion: The RBC scheme is a widely adopted control strategy in various buildings due to its simplicity in implementation. The RBC-SB is

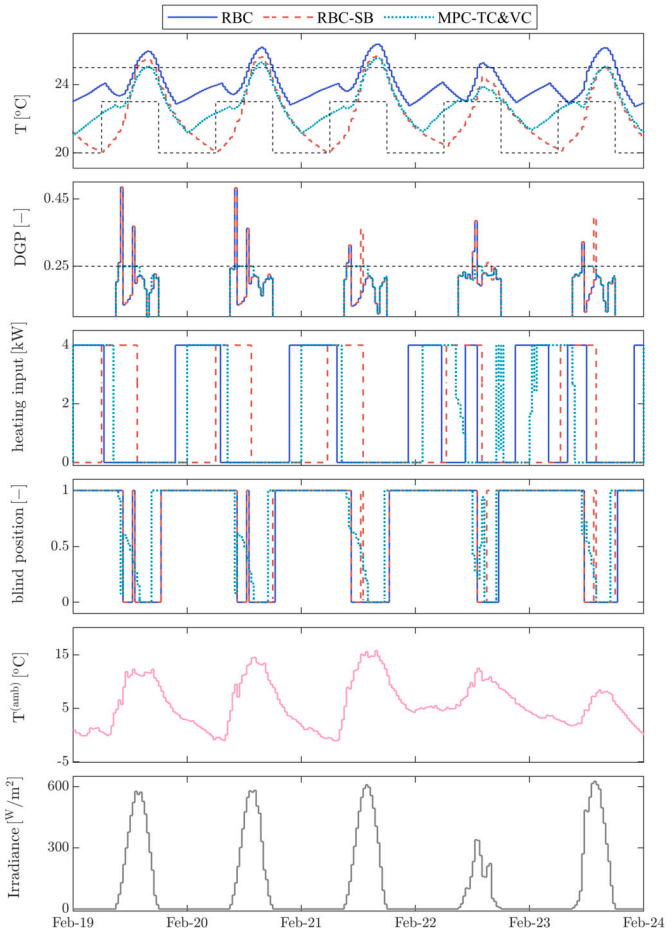

Fig. 7. The figure shows the room temperatures and DGP resulting from different controllers taking into account thermal and visual comfort. The dashed line represents time-varying constraints that affect the controllers with the setback. The bound for visual comfort is $DGP_{max} = 0.25$. Furthermore, the respective control inputs, ambient temperature, and solar radiation are shown.

a modified version of RBC that incorporates a lower temperature range during night-time operation, with the objective of improving energy efficiency. As a consequence, the RBC-SB leads to reduced energy consumption at the cost of more violations of the temperature lower bound. Furthermore, the lower room temperature during the night results in fewer instances of the upper temperature bound being exceeded. Utilizing MPC-TC&VC, the MPC algorithm proposed in this study, leads to dynamic adjustment of control inputs to optimize energy consumption while maintaining not only the thermal comfort constraints but also the visual comfort ones. This approach ensures improved comfort levels for the occupants in terms of temperature and visual conditions. It is worth noting that all the mentioned controllers exhibit minor violations in terms of DGP (compare the bottom-right of Fig. 7 with Fig. 9, which demonstrates the performance for different MPC schemes). Nonetheless, one can see that MPC-TC&VC outperforms RBC and RBC-SB controllers in terms of DGP violations, which is potentially due to the utilization of a reliable model for DGP prediction in MPC-TC&VC. Similarly, it is evident that MPC-TC&VC demonstrates fewer violations of thermal con-

Table 4
Performance comparison for different configurations of MPC implementation.

	Method Acronym	Energy Consumption [kWh]	Thermal UB Violation [Kh]	Thermal LB Violation [Kh]	Visual Violation [h/day]	Blind Closed [h]
MPC with thermal comfort constraints and without blind control	MPC-NB	1089	153	16.8	3.48	0
MPC with thermal comfort constraints	MPC-TC	1551	8.52	50.8	0.80	125
MPC with thermal and visual comfort constraints	MPC-TC&VC	1663	7.45	49.9	0.07	146
MPC with visual comfort and thermal lower bound constraints	MPC-VC&TLB	1585	44.0	34.8	0.07	93

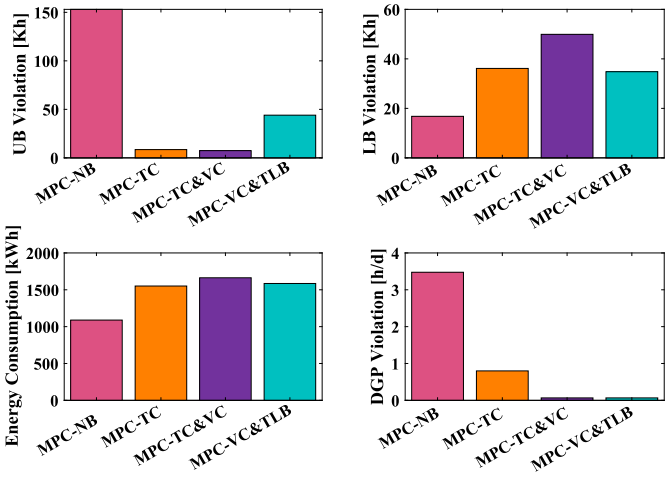

Fig. 8. Performance comparison for different configurations of MPC implementation.

straints compared to RBC and RBC-SB, benefiting from incorporating a suitable model for the thermal dynamics of the building in MPC-TC&VC. Thus, since MPC-TC&VC employs reliable models for the thermal dynamics of the building and DGP, it can effectively maintain thermal and visual comfort at the cost of slightly extra energy consumption. The increased energy consumption is due to the more frequently closed blinds, which reduces solar gains and makes it more costly for the MPC-TC&VC to satisfy the lower bound on room temperature.

5.2. MPC implementation: the impact of blinds and visual comfort considerations

To gain a deeper understanding of the impact of visual comfort consideration and the subsequent potential roles of the blinds on the MPC implementation, we compare MPC-TC&VC with the following MPC schemes:

- *MPC with thermal comfort constraints and without blind control* (MPC-NB): In this case, our focus lies on the MPC control of the thermal dynamics of the building; meanwhile, it is assumed that the windows in the zone under consideration are not equipped with shades or blinds, i.e., the zone receives the full extent of solar radiation during daytime.
- *MPC with thermal comfort constraints* (MPC-TC): This case involves MPC implementation for the heating system of the zone, where the windows are equipped with controlled blinds, and MPC is required to maintain the thermal comfort constraints.
- *MPC with thermal comfort and temperature lower bound constraints* (MPC-VC&TLB): This case is similar to the MPC-TC&VC, but with relaxed upper bounds on the zone temperature.

Table 4 and Fig. 8 compare the control performance for the schemes mentioned above. Additionally, Fig. 9 illustrates the temperature within the room and the amount of perceived glare throughout a span of five days, demonstrating the results obtained from implementing the above control schemes.

Discussion: Each of the mentioned MPC schemes is able to optimize energy consumption while maintaining the intended comfort conditions under the presumed operational constraints and using the developed model for thermal dynamics of the building. The MPC-NB scenario is specifically considered to explore and examine the implications of not incorporating blind control within the MPC framework and evaluate the effectiveness of thermal comfort constraints in such situations. The MPC-TC scheme is the current MPC benchmark configuration in the literature, aiming to optimize the overall system performance in terms of energy consumption and taking into account the thermal comfort requirements and the regulation of the solar radiation impact through controlling the blinds. On the other hand, MPC-TC&VC, the MPC approach proposed in this study, additionally considers visual comfort constraints. The MPC-VC&TLB scheme is a slightly modified version of MPC-TC&VC proposed to investigate the compromise between the visual comfort and energy consumption. More precisely, the distinguishing factor of MPC-VC&TLB is the absence of an upper bound on thermal comfort. Consequently, this scheme prioritizes visual comfort, i.e., it neglects thermal comfort by allowing upper constraint violations and only trades-off visual comfort with energy consumption by primarily focusing on closing the blinds to regulate the amount of incoming solar radiation, ensuring a visually comfortable environment while not enforcing a specific upper-temperature limit for thermal comfort. Comparing the above MPC configurations, one can observe the consequent inherent trade-offs between maintaining comfort conditions and energy consumption. Specifically, reducing violations of the thermal bounds and DGP constraints leads to increased energy consumption. The observed phenomenon is due to the primary mechanism employed to mitigate these violations, namely the utilization of blinds to obstruct solar radiation, a cost-free energy source. More precisely, the decrease in received solar heat necessitates the heating system of the building to compensate, and consequently, it leads to increased energy consumption. As a result, the MPC-NB implementation demonstrates the lowest energy consumption while exhibiting the highest comfort violations. On the other hand, in the cases of MPC-TC and MPC-TC&VC, the blinds are utilized to maintain thermal comfort, resulting in additional energy consumption, which is slightly increased in the MPC-TC&VC scheme due to the additional consideration of visual comfort constraints. More precisely, MPC-TC&VC ensures both thermal and visual comfort constraints satisfaction at the expense of 7.2% more energy consumption compared to MPC-TC, which is the benchmark MPC configuration. Compared to MPC-TC&VC, the modification in MPC-VC&TLB leads to a reasonably reduced energy consumption and a minor increase in violations of thermal upper bound while retaining the same reduced DGP violation and less frequently closed blinds. Consequently, employing the MPC-VC&TLB scheme results in maintaining DGP violation levels comparable to MPC-TC&VC, and energy consumption levels similar to MPC-TC, namely less than 2.2% extra energy consumption compared to the benchmark MPC configuration. Accordingly, the MPC-VC&TLB scheme can be regarded as a potential trade-off between thermal and visual comfort constraints and energy consumption.

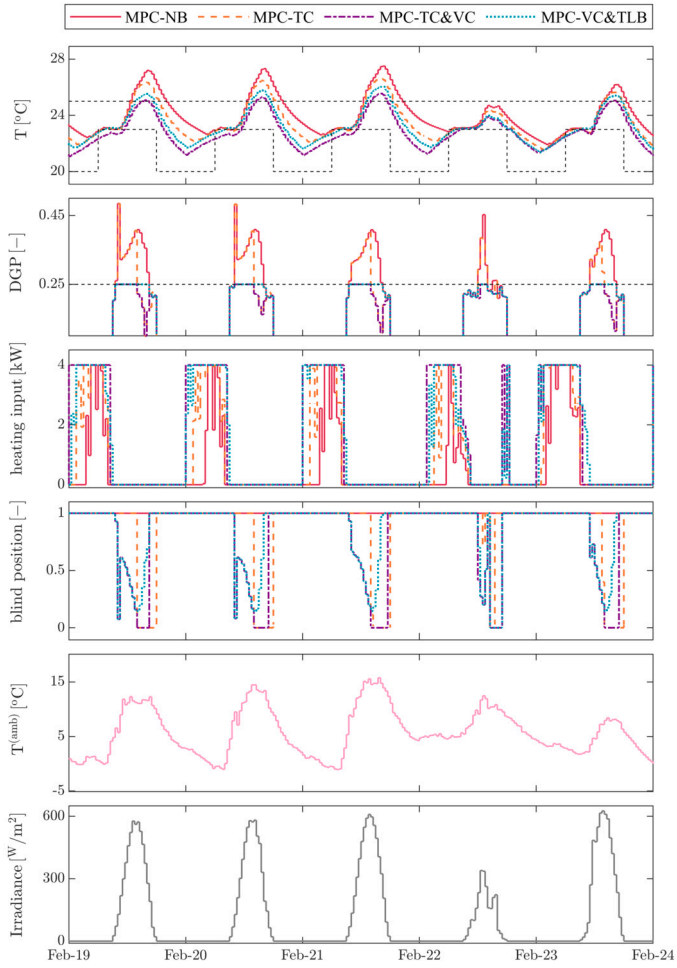

Fig. 9. The figure shows the room temperatures and DGP resulting from different MPC configurations. For thermal comfort, the dashed line represents time-varying constraints that affect the controllers with the setback. The bound for visual comfort is $DGP_{max} = 0.25$. Furthermore, the respective control inputs, ambient temperature, and solar radiation are shown.

6. Conclusion and future work

In this paper, a Model Predictive Control (MPC) scheme with thermal and visual comfort constraints was developed. The thermal dynamics of the building are modeled using a linear auto-regressive exogenous model. The visual comfort, measured in terms of Daylight Glare Probability (DGP), is modeled using a semi-linear support vector regression model. The MPC approach was then applied to a simulated setup of a radiant-based heating system and Venetian blinds in an environment modeled based on a real-world office building. In order to evaluate the resulting performances, the proposed MPC strategy is compared to various rule-based control (RBC) and alternative MPC approaches. Comparing the results confirms that the proposed MPC scheme effectively decreases the overall costs in terms of energy consumption while retaining thermal and visual comfort. Furthermore, it was observed that visual discomfort commonly occurs around the time of peak solar radiations, causing excessive glare and also resulting in heating the room. Consequently, imposing constraints on DGP partially limits the room temperature, and thus, one can relax thermal upper bounds and only incorporate DGP constraints. While the proposed MPC schemes consider thermal comfort, they also ensure the satisfaction of the visual comfort constraints at the expense of 2.2% to 7.2% higher energy consumption compared to the benchmark MPC configuration.

While the MPC schemes developed in this paper have been validated and compared with other methods through an extensive numerical case study, subsequent research may focus on their verification in practical settings and on the actual real-world system. Furthermore, the performance and scalability of the proposed control methodology can be evaluated on large-scale buildings with a higher number of zones in future research works. Moreover, there is potential for extending the proposed MPC formulation to ensure sufficient illuminance in the workspace additionally.

Declaration of competing interest

The authors declare that they have no known competing financial interests or personal relationships that could have appeared to influence the work reported in this paper.

Data availability

Data will be made available on request.

Acknowledgement

We would like to thank Prof. Kristina Orehounig and Prof. John Lygeros for their invaluable help and support throughout this research. In addition, we would like to express our gratitude to Felix Bünning, Ali Motamed, Marta Benedetti, and Massimo Fiorentini for the productive and insightful discussions that contributed to the development of our research. Additionally, we would like to thank Reto Fricker and Sascha

Stoller for sharing their knowledge and providing assistance throughout the implementation process. Finally, we appreciate Yannic Trüb's cooperation and patience in allowing us to conduct our experiments in his office.

Appendix A. Identification of building thermal dynamics

To identify the thermal dynamics of the building, the coefficients of ARX model (10) need to be estimated. To this end, we define vector θ as

$$\theta := [\theta_T^\mathsf{T}, \theta^{(\text{amb})\mathsf{T}}, \theta^{(\text{adj},1)\mathsf{T}}, \dots, \theta^{(\text{adj},N_{\text{adj}})\mathsf{T}}, \theta^{(\text{sol})\mathsf{T}}, \theta^{(\text{heat})\mathsf{T}}]^\mathsf{T},$$

where θ_T, $\theta^{(\text{amb})}$, $\theta^{(\text{adj},1)}$, $\dots$, $\theta^{(\text{adj},N_{\text{adj}})}$, $\theta^{(\text{sol})}$, and $\theta^{(\text{heat})}$ are the following vectors

$$\begin{aligned}
\theta_T &:= [\theta_0, \dots, \theta_{n_T}]^\mathsf{T},\\
\theta^{(\text{amb})} &:= [\theta_0^{(\text{amb})}, \dots, \theta_{n_{\text{amb}}}^{(\text{amb})}]^\mathsf{T},\\
\theta^{(\text{adj},i)} &:= [\theta_0^{(\text{adj},i)}, \dots, \theta_{n_{\text{adj},i}}^{(\text{adj},i)}]^\mathsf{T}, \quad \forall\, i = 1, \dots, N_{\text{adj}},\\
\theta^{(\text{sol})} &:= [\theta_0^{(\text{sol})}, \dots, \theta_{n_{\text{sol}}}^{(\text{sol})}]^\mathsf{T},\\
\theta^{(\text{heat})} &:= [\theta_0^{(\text{heat})}, \dots, \theta_{n_{\text{heat}}}^{(\text{heat})}]^\mathsf{T}.
\end{aligned}$$

Furthermore, given the measurement data

$$\mathscr{M} := \left\{ (T_k, T_k^{(\text{amb})}, T_k^{(\text{adj},1)}, \dots, T_k^{(\text{adj},N_{\text{adj}})}, \dot{Q}_k^{(\text{sol})}, \dot{Q}_k^{(\text{heat})}) \;\middle|\; k = 0, \dots, n_{\mathscr{M}} \right\},$$

we define vector φ_k as

$$\begin{aligned}
\varphi_k := [&T_k, \dots, T_{k-n_T}, T_k^{(\text{amb})}, \dots, T_{k-n_{\text{amb}}}^{(\text{amb})},\\
&T_k^{(\text{adj},1)}, \dots, T_{k-n_{\text{adj},1}}^{(\text{adj},1)}, T_k^{(\text{adj},2)}, \dots, T_{k-n_{\text{adj},1}}^{(\text{adj},2)}, \dots, T_k^{(\text{adj},N_{\text{adj}})}, \dots, T_{k-n_{\text{adj},N_{\text{adj}}}}^{(\text{adj},N_{\text{adj}})},\\
&\dot{Q}_k^{(\text{sol})}, \dots, \dot{Q}_{k-n_{\text{sol}}}^{(\text{sol})}, \dot{Q}_k^{(\text{heat})}, \dots, \dot{Q}_{k-n_{\text{heat}}}^{(\text{heat})}]^\mathsf{T},
\end{aligned}$$

for $n_{\text{lag}} \le k \le n_{\mathscr{M}} - 1$, where n_{lag} denotes the value of largest lag considered in the ARX model (10), i.e., $n_{\text{lag}} := \max\{n_T, n_{\text{adj},1}, \dots, n_{\text{adj},N_{\text{adj}}}, n_{\text{sol}}, n_{\text{heat}}\}$. Accordingly, (10) implies that

$$T_{k+1} = \varphi_k^\mathsf{T}\theta + e_k,$$

for $k = n_{\text{lag}}, \dots, n_{\mathscr{M}} - 1$. Thus, we can obtain θ through solving the following least square problem

$$\hat{\theta} := \underset{\theta}{\text{argmin}} \sum_{k=n_{\text{lag}}}^{n_{\mathscr{M}}-1} (T_{k+1} - \varphi_k^\mathsf{T}\theta)^2,$$

which estimates θ as the vector of coefficients minimizing sum of squared one-step ahead prediction errors for the ARX model (10). For the SolAce, due to well insulation of the walls, the terms related to the impact of adjacent units are disregarded.

References

[1] International Energy Agency (IEA), Building Energy Performance Metrics, 2015.
[2] S. Brasche, W. Bischof, Daily time spent indoors in German homes – baseline data for the assessment of indoor exposure of German occupants, Int. J. Hyg. Environ. Health 208 (2005) 247–253.
[3] Y. Al Horr, M. Arif, A. Kaushik, A. Mazroei, M. Katafygiotou, E. Elsarrag, Occupant productivity and office indoor environment quality: a review of the literature, Build. Environ. 105 (2016) 369–389.
[4] A. Afram, F. Janabi-Sharifi, Theory and applications of HVAC control systems–a review of model predictive control (MPC), Build. Environ. 72 (2014) 343–355.
[5] D. Sturzenegger, D. Gyalistras, M. Morari, R.S. Smith, Model predictive climate control of a Swiss office building: implementation, results, and cost–benefit analysis, IEEE Trans. Control Syst. Technol. 24 (2016) 1–12.
[6] M. Castilla, J. Álvarez, J. Normey-Rico, F. Rodríguez, Thermal comfort control using a non-linear MPC strategy: a real case of study in a bioclimatic building, J. Process Control 24 (2014) 703–713.
[7] E. Žáčeková, Z. Váňa, J. Cigler, Towards the real-life implementation of MPC for an office building: identification issues, Appl. Energy 135 (2014) 53–62.
[8] T. Hilliard, L. Swan, Z. Qin, Experimental implementation of whole building MPC with zone based thermal comfort adjustments, Build. Environ. 125 (2017) 326–338.
[9] J. Široký, F. Oldewurtel, J. Cigler, S. Prívara, Experimental analysis of model predictive control for an energy efficient building heating system, Appl. Energy 88 (2011) 3079–3087.
[10] F. Oldewurtel, A. Parisio, C.N. Jones, D. Gyalistras, M. Gwerder, V. Stauch, B. Lehmann, M. Morari, Use of model predictive control and weather forecasts for energy efficient building climate control, Energy Build. 45 (2012) 15–27.
[11] J. Drgoňa, J. Arroyo, I.C. Figueroa, D. Blum, K. Arendt, D. Kim, E.P. Ollé, J. Oravec, M. Wetter, D.L. Vrabie, et al., All you need to know about model predictive control for buildings, Annu. Rev. Control 50 (2020) 190–232.
[12] F. Smarra, A. Jain, T. de Rubeis, D. Ambrosini, A. D'Innocenzo, R. Mangharam, Data-driven model predictive control using random forests for building energy optimization and climate control, Appl. Energy 226 (2018) 1252–1272.
[13] F. Bünning, B. Huber, P. Heer, A. Aboudonia, J. Lygeros, Experimental demonstration of data predictive control for energy optimization and thermal comfort in buildings, Energy Build. 211 (2020).
[14] B. Huber, F. Bünning, A. Decoussemaeker, P. Heer, J. Lygeros, Benchmarking of data predictive control in real-life apartment during heating season, J. Phys. Conf. Ser. 2042 (2021) 012024, IOP Publishing.
[15] M. Khosravi, A. Eichler, A. Aboudonia, R. Buck, R.S. Smith, Data-driven predictive control of buildings; a regression based approach, in: 2019 IEEE Conference on Control Technology and Applications (CCTA), IEEE, 2019, pp. 605–610.
[16] N. Lefebure, M. Khosravi, M.H. Badyn, F. Bünning, J. Lygeros, C. Jones, R.S. Smith, Distributed model predictive control of buildings and energy hubs, Energy Build. 259 (2022) 111806.
[17] J. Xie, A.O. Sawyer, Simulation-assisted data-driven method for glare control with automated shading systems in office buildings, Build. Environ. 196 (2021) 107801.
[18] G. Chiesa, D. Di Vita, A. Ghadirzadeh, A.H.M. Herrera, J.C.L. Rodriguez, A fuzzy-logic IoT lighting and shading control system for smart buildings, Autom. Constr. 120 (2020) 103397.
[19] A. Motamed, B. Bueno, L. Deschamps, T.E. Kuhn, J.-L. Scartezzini, Self-commissioning glare-based control system for integrated venetian blind and electric lighting, Build. Environ. 171 (2020) 106642.
[20] R.J. De Dear, G.S. Brager, Thermal comfort in naturally ventilated buildings: revisions to ASHRAE standard 55, Energy Build. 34 (2002) 549–561.
[21] F. Isaia, M. Fiorentini, V. Serra, A. Capozzoli, Enhancing energy efficiency and comfort in buildings through model predictive control for dynamic façades with electrochromic glazing, J. Build. Eng. 43 (2021) 102535.
[22] J. Wienold, J. Christoffersen, Evaluation methods and development of a new glare prediction model for daylight environments with the use of CCD cameras, Energy Build. 38 (2006) 743–757.
[23] S. Yang, M.P. Wan, B.F. Ng, S. Dubey, G.P. Henze, W. Chen, K. Baskaran, Model predictive control for integrated control of air-conditioning and mechanical ventilation, lighting and shading systems, Appl. Energy 297 (2021) 117112.
[24] L. Ljung, System Identification: Theory for the User, Prentice Hall, 1999.
[25] A. Motamed, L. Deschamps, J.-L. Scartezzini, On-site monitoring and subjective comfort assessment of a sun shadings and electric lighting controller based on novel High Dynamic Range vision sensors, Energy Build. 149 (2017) 58–72.
[26] P. Richner, P. Heer, R. Largo, E. Marchesi, M. Zimmermann, NEST–una plataforma para acelerar la innovación en edificios, Inf. Constr. 69 (2017) e222–e222.
[27] T. Hastie, R. Tibshirani, J.H. Friedman, J.H. Friedman, The Elements of Statistical Learning: Data Mining, Inference, and Prediction, vol. 2, Springer, 2009.
[28] C. Cortes, V. Vapnik, Support-vector networks, Mach. Learn. 20 (1995) 273–297.